Optical polar OFDM: on the effect of time-domain power allocation under power and dynamic-range constraints*

H. Elgala, S.K. Wilson, and T.D.C. Little†

January 07, 2015

MCL Technical Report No. 01-07-2015

Abstract–Polar OFDM (P-OFDM) is an OFDM format that can double the spectral efficiency of existing real-valued and unipolar optical OFDM intensity-modulation with direct detection (IM/DD) optical communication systems. P-OFDM modulates the amplitude and phase of a complex OFDM signal to allow a real unipolar signal. In this paper, we investigate the effect of power allocation to the phase and the amplitude components of P-OFDM time-domain signal on (1) the effective signal-to-noise ratio (SNR) at the receiver (2) the peak-to-average power ratio (PAPR) under transmit power constraint and (3) the induced clipping noise under optical-source's dynamic-range and transmit power constraints. In addition to a 4 dB reduction in PAPR from ACO-OFDM, we demonstrate the improvement of throughput for P-OFDM over other optical OFDM methods when the signal power is limited.

Keywords: OFDM, IM/DD, Polar, VLC, Li-Fi, LEDs, Clipping.

*In *Proc. IEEE WCNC 2015, 2015 IEEE Wireless Communications and Networking Conference (WCNC) - Track 1: PHY and Fundamentals*, 2015. This work is supported by the NSF under grant No. EEC-0812056. Any opinions, findings, and conclusions or recommendations expressed in this material are those of the author(s) and do not necessarily reflect the views of the National Science Foundation.

†H. Elgala and T.D.C. Little are with the Department of Electrical and Computer Engineering, Boston University, Boston, Massachusetts, {*helgala, tdcl*}*@bu.edu*. S.K. Wilson is with the Electrical Engineering Department, Santa Clara University, Santa Clara, CA, 95053, USA, *skwilson@scu.edu*.

1 Introduction

The increased demand for mobile computing and the accompanying need for higher data rates is stressing current and future wireless communications systems. Services providing continuous streaming (*e.g.*, video) and constant cloud connectivity (*e.g.*, cloud file synchronization) are particularly onerous on data capacity requirements. Technologies such as fiber optics [1] can increase transmission along part of the network delivery path, the limited capacity of existing wireless local area networks (WLANs) can severely limit transmission rates within the home or office. To keep up with increasing data rate requirements, we explore opportunities for new, unexploited channels of data delivery. One such method is optical wireless communications (OWC). With OWC, light-emitting diodes (LEDs) or laser diodes (LDs) can be used to modulate light. In the former, LEDs can serve a dual role in providing lighting and data communication in an energy efficient way based on the visible light communications (VLC) or the Li-Fi technology [2].

A simple low-cost way to implement OWC is by intensity-modulation (IM) with direct detection (DD). IM/DD systems require a modulation signal that is real and positive (*i.e.* unipolar). OFDM provides a flexible way to implement high data rate systems in OWC. However, OFDM is inherently a pass-band system with a complex baseband output. Several methods to modulate IM/DD systems with OFDM have been proposed, including ACO-OFDM [3] and DC-biased optical OFDM (DCO-OFDM) [4]. However though ACO-OFDM is energy efficient it only uses half the bandwidth, *i.e.* DC-biased OFDM uses the full available bandwidth, but is energy-inefficient due to the DC-biasing.

In VLC, and due to the limit on power consumption, eye safety regulation and dimming requirement, the system usually operates under some average optical transmit power constraint [5]. In addition, the dynamic-range limitation of an LED require methods that have low peak-to-average power ratio (PAPR) to avoid clipping noise [6–8]. Though formats such as Flip-OFDM [9] or position modulation OFDM (PM-OFDM) [10] address the PAPR issue, they still only use half the available bandwidth.

A recently proposed optical OFDM format, called polar OFDM (P-OFDM), is both energy- and spectrally-efficient for direct IM/DD systems [11, 12]. P-OFDM offers twice the data rate of ACO-OFDM while maintaining low PAPR and high energy efficiency. The basic idea is to modulate an OFDM signal with quadrature amplitude modulation (QAM) symbols, X_k, on all N sub-carriers, *i.e.* similar to RF-OFDM signal generation. Rather than to transmit the complex OFDM samples x_n, one transmits, after a Cartesian-to-Polar operation, the amplitude r_n and the phase θ_n over two consecutive periods. As θ_n is uniformly distributed between 0 and 2π, for at least half the signal power, the PAPR is low which is beneficial in a system that has transmit power and LED dynamic-range limitations. This modulation method has twice the rate of ACO-OFDM and the other methods based on it and is more energy efficient than DCO-OFDM.

The remainder of this paper is organized as follows. The generation of the P-OFDM signal and the demodulation process are highlighted in Section II. In Section III, and under the nonlinear coordinate transformation (Cartesian-to-Polar and Polar-to-Cartesian operations) applied on the complex samples, the noise and the effective signal-to-noise ratio (SNR) at the receiver are analyzed. In Section IV, and based on simulation results, the achieved system performance in terms of PAPR, induced clipping noise and bit-error rate (BER) under fixed power and dynamic-range constraints are presented. Conclusions are drawn in Section V.

2 The optical polar OFDM system

As shown in Fig. 1, the P-OFDM signal is obtained based on adding Cartesian-to-Polar and Polar-to-Cartesian operations to the conventional RF-OFDM communication chain. The N complex samples forming an OFDM symbol (x_n), after N-points complex inverse fast Fourier transform (IFFT) operation, are described by,

$$x_n = \frac{1}{\sqrt{N}} \sum_{k=0}^{N-1} X_k \exp^{(j\frac{2\pi}{N}nk)} \tag{1}$$

where, $n = 0, \cdots, N-1$ and $k = 0, \cdots, N-1$.

The time-domain output samples x_n are input to the Cartesian-to-Polar operation. The N amplitudes of the different samples ($|x_n| = r_n$) and the N phases of the different samples ($\arg(x_n) = \theta_n$) are transmitted (electrical-to-optical conversion, E/O) during two consecutive periods, *i.e.* P-OFDM symbol.

After the optical-to-electrical conversion, O/E, the received samples containing the amplitudes and phases of the transmitted samples ($r_n^{'}$), ($\theta_n^{'}$), respectively are converted from polar to the Cartesian coordinates of the original OFDM signal. We denote the reconstructed Cartesian coordinates $y_k = r^{'}n\exp(j\theta_n^{'})$ and the fast Fourier transform (FFT) of the reconstructed values Y_k. The FFT values Y_k contain noisy versions of the original transmitted QAM symbols. However, due to the non-linearity of the conversion process, the noise affecting the demodulation of the symbols is not additive noise anymore. In section 3 we evaluate the effect of polar-to-Cartesian coordinate conversion on the received additive white Gaussian noise.

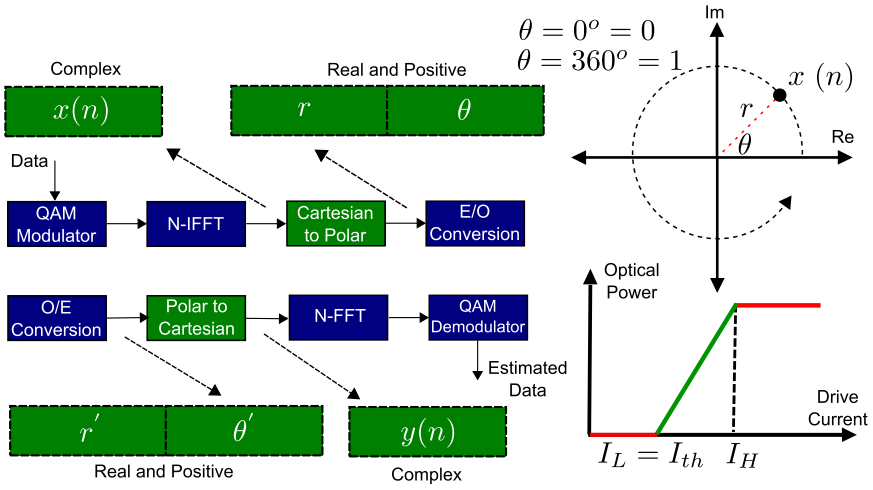

Figure 1: The P-OFDM system. Polar coordinates: $\theta = 0$ is mapped to value 0 (associated to I_{L}) while $\theta = 360^o$ is mapped to value 1 (associated to I_{H}). The LED drive current vs. optical power: I_{L} is the minimum drive current (threshold or turn-on current) and I_{H} is the maximum allowed drive current. All real-valued signals are constrained by the dynamic range of the LED, $\mathrm{DR_{LED}} = I_{\mathrm{H}} - I_{\mathrm{L}}$. As a result, the OFDM signal is vulnerable to nonlinear baseband distortion, *i.e.* mainly clipping.

At a fixed average power per P-OFDM symbol $\mathrm{P_s} = 15\mathrm{dBm}$ (the average energy of x_n is the same as the average energy of the constellations/subcarriers X_k), Fig. 2 shows the normalized time-domain samples of a single P-OFDM symbol using 4-bits (16-QAM) per sub-carrier. Regardless

of the modulation order, the envelope of the θ_n samples is confined between 0 ($\theta_n = 0^o$) and 1 ($\theta_n = 360^o$).

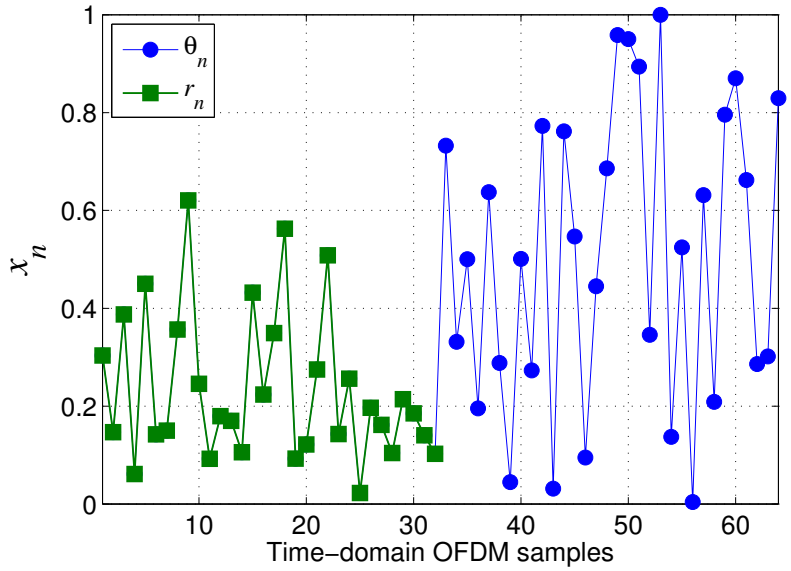

Figure 2: Normalized time-domain of one P-OFDM symbol (32 samples).

3 Noise and effective SNR analysis

For large number of sub-carriers, and according to the central limit theorem, the complex OFDM samples in Eq. (1) can be accurately modeled as a complex Gaussian random process with a zero mean value $\mu_x = 0$ and a variance σ_x^2. $\mathrm{P_s}$ is equal to σ_x^2 for $\mu_x = 0$. Thus in the polar coordinates, the distribution of r_n is a Rayleigh distribution and θ_n is uniformly distributed between 0 and 2π. Accordingly, μ_r is the mean of r_n and μ_θ is the mean of θ, given by,

$$\mu_r = \sigma_x \sqrt{\frac{\pi}{2}} \tag{2}$$

$$\mu_\theta = \pi \tag{3}$$

Having $k_1|x_n| = k_1 r_n$ and $k_2 \mathrm{arg}(x_n) = k_2\theta_n$ in radians, where k_1 and k_2 are scaling factors that control the relative transmit power of the two parts of the P-OFDM symbol, DR_r is the dynamic range of the P-OFDM signal representing r_n, *i.e.* $(k_1 r_n)$ and DR_θ is the dynamic range of the P-OFDM signal representing θ_n, *i.e.* $(k_2\theta_n)$. To ensure that DR_r and DR_θ stay within $\mathrm{DR_{LED}}$ (see Fig. 1), the greatest value of k_1 and k_2 are,

$$k_1 = \frac{\mathrm{DR_{LED}}}{\max\{r_n\}} = \frac{I_\mathrm{H} - I_\mathrm{L}}{\max\{r_n\}} \tag{4}$$

$$k_2 = \frac{\mathrm{DR_{LED}}}{\max\{\theta_n\}} = \frac{I_\mathrm{H} - I_\mathrm{L}}{\max\{\theta_n\}} \tag{5}$$

The overall channel impulse response including the O/E and E/O conversion are assumed to be non-dispersive with an amplitude of 1. Accordingly, the received P-OFDM signal can be described as:

$$y_n^{\mathrm{S}}(t) = \begin{cases} r_n^{'} = k_1 r_n + z_n, & 0 \le t < T_{\mathrm{OFDM}}/2 \\ \theta_n^{'} = k_2 \theta_n + z_{n+N/2}, & T_{\mathrm{OFDM}}/2 \le t < T_{\mathrm{OFDM}} \end{cases} \tag{6}$$

where, z_n is the additive white Gaussian noise (AWGN) during r_n, $z_{n+N/2}$ is the AWGN during θ_n and T_{OFDM} is the two consecutive P-OFDM symbol periods.

From Eq. (2) and Eq. (3), the SNR of the received P-OFDM signal is given by,

$$\mathrm{SNR}^{\mathrm{S}} = \frac{k_1 \sigma_x \sqrt{\pi/2} + k_2 \pi}{\sigma_z^2} = \frac{k_1 \sqrt{\mathrm{P_s} \pi/2} + k_2 \pi}{\sigma_z^2} \tag{7}$$

where, the instantaneous signal power represents the modulated LEDs' intensity, *i.e.* modulated drive current, and σ_z^2 is the AWGN noise power.

In the polar-coordinates, the reconstructed P-OFDM samples are described as:

$$\begin{aligned} y_n^{\mathrm{P}} &= r_n^{'} e^{j\theta_n^{'}} \\ &= (k_1 r_n + z_n) e^{j(k_2 \theta_n + z_{n+N/2})} \\ &= k_1 r_n e^{j\theta_n} e^{j\frac{z_{n+N/2}}{k_2}} + z_n e^{j(\theta_n + \frac{z_{n+N/2}}{k_2})} \end{aligned} \tag{8}$$

From Eq. (8), there are two sources of noise: multiplicative noise, $e^{j\frac{z_{n+N/2}}{k_2}}$ and additive noise, $z_n e^{j(\theta_n + \frac{z_{n+N/2}}{k_2})}$. If k_2 is assumed large enough, the angle noise is negligible, *i.e.* $e^{j\frac{z_{n+N/2}}{k_2}} \approx 1$. In this case:

$$y_n^{\mathrm{P}} \approx k_1 x_n + z_n e^{j\theta_n} \tag{9}$$

and the SNR of the reconstructed P-OFDM signal is given by,

$$\mathrm{SNR}^{\mathrm{P}} \approx \frac{k_1^2 \sigma_{\mathrm{x}}^2}{\sigma_{\mathrm{z}}^2} \approx \frac{k_1^2 \mathrm{P_s}}{\sigma_{\mathrm{z}}^2} \tag{10}$$

Here, the performance is solely controlled by k_1. Accordingly, the θ_n samples should be large enough to ensure that the multiplicative noise is diminished, but more power should be allocated to the r_n samples to maximize $\mathrm{SNR}^{\mathrm{P}}$.

Assuming $\frac{z_{n+N/2}}{k_2}$ is small enough, so that,

$$e^{j(\theta_n + \frac{z_{n+N/2}}{k_2})} \approx e^{j\theta_n}(1 + j\frac{z_{n+N/2}}{k_2}) \tag{11}$$

Therefore,

$$\begin{aligned} y_n^{\mathrm{P}} &\approx k_1 x_n (1 + j\frac{z_{n+N/2}}{k_2}) + z_n e^{j\theta_n}(1 + j\frac{z_{n+N/2}}{k_2}) \\ &= k_1 x_n + j\frac{k_1}{k_2} z_{n+N/2} x_n + z_n e^{j\theta_n} + j\frac{z_n z_{n+N/2}}{k_2} e^{j\theta_n} \\ &\approx k_1 x_n + j\frac{k_1}{k_2} z_{n+N/2} x_n + z_n e^{j\theta_n} \end{aligned} \tag{12}$$

where, again k_2 is assumed large enough to ignore $j\frac{z_n z_{n+N/2}}{k_2}e^{j\theta_n}$. Accordingly,

$$\mathrm{SNR}^{\mathrm{P}} = \frac{k_1^2\sigma_{\mathrm{x}}^2}{\sigma_{\mathrm{z}}^2(1+\frac{\mathrm{P_s}k_1^2}{k_2^2})} = \frac{\mathrm{P_s}}{\sigma_{\mathrm{z}}^2(\frac{1}{k_1^2}+\frac{\mathrm{P_s}}{k_2^2})} \tag{13}$$

Taking the ratio of $\mathrm{SNR}^{\mathrm{P}}$ and $\mathrm{SNR}^{\mathrm{S}}$ to describe the relationship between the amount of transmitted power and the effective SNR at the demodulator, we find:

$$\begin{aligned}\rho = \frac{\mathrm{SNR}^{\mathrm{P}}}{\mathrm{SNR}^{\mathrm{S}}} &= \frac{\frac{\mathrm{P_s}}{\sigma_z^2(\frac{1}{k_1^2}+\frac{\mathrm{P_s}}{k_2^2})}}{\frac{k_1\sqrt{\mathrm{P_s}\pi/2}+k_2\pi}{\sigma_z^2}} \\ &= \frac{\mathrm{P_s}}{(\frac{1}{k_1^2}+\frac{\mathrm{P_s}}{k_2^2})(k_1\sqrt{\mathrm{P_s}\pi/2}+k_2\pi)}\end{aligned} \tag{14}$$

Letting $k_1 = \alpha k_2$, we have:

$$\begin{aligned}\rho &= \frac{\mathrm{P_s}}{\frac{1}{k_2^2}(\mathrm{P_s}+\frac{1}{\alpha^2})k_2(\alpha\sqrt{\mathrm{P_s}\pi/2}+\pi)} \\ &= \frac{k_2\alpha^2\mathrm{P_s}}{(1+\mathrm{P_s}\alpha^2)(\alpha\sqrt{\mathrm{P_s}\pi/2}+\pi)} \\ &= \frac{k_2\alpha^2\mathrm{P_s}}{(\alpha\sqrt{\mathrm{P_s}\pi/2}+\pi+\alpha^3\sqrt{\mathrm{P_s}^3\pi/2}+\mathrm{P_s}\alpha^2\pi)}\end{aligned} \tag{15}$$

Equation (15) for $\mathrm{P_s} = 1$ and different values of α and k_2 is plotted in Fig. 3. The power allocation to the r_n and θ_n samples through k_1 and k_2 is important to achieve the SNR required to fulfil a target bit-error performance, *i.e.* $k_1 > k_2$ is recommended as shown in Fig. 3. For this specific value of $\mathrm{P_s} = 1$, $\alpha = 1.9$ is the optimum value to maximize ρ.

4 Simulation results

Using Monte Carlo simulation, and at fixed $\mathrm{DR_{LED}}$ and $\mathrm{P_s}$, we show how k_1 and k_2 also control the PAPR. Moreover, assuming AWGN of -15dBm (typical optical receiver sensitivity) and perfect synchronization between the transmitter and the receiver, the influence of $\mathrm{DR_{LED}}$ on the induced clipping noise power and BER performance curves of a P-OFDM system are presented, *i.e.* also compared to a ACO-OFDM system. $\mathrm{DR_{LED}}$ is quantified by the value of the clipping ratio. The clipping ratio is defined in dB as,

$$\text{Clipping Ratio (dB)} = 10\log_{10}\frac{\mathrm{DR_{LED}}}{\mathrm{P_s}} \tag{16}$$

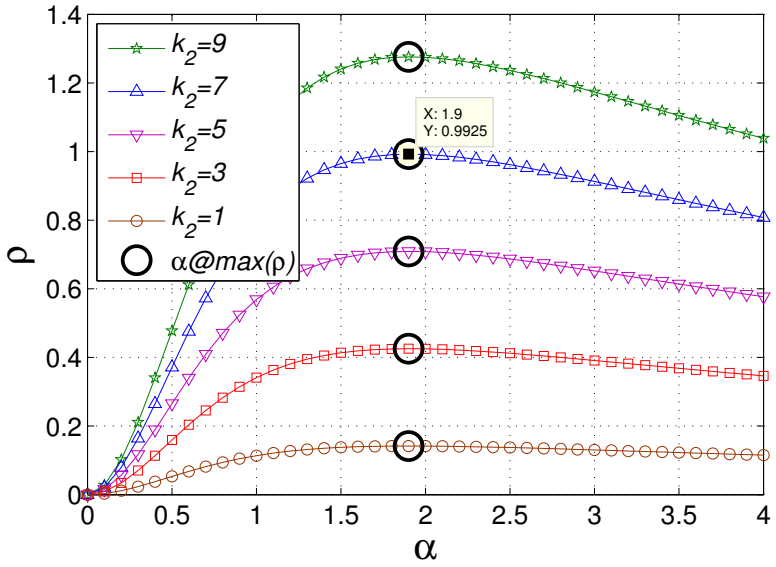

Figure 3: Plot of ρ, the ratio of the SNR of the reconstructed P-OFDM signal to the received SNR as a function of α, where α is the ratio of the scaling factor of the θ_n samples, k_2 to the scaling factor of the r_n samples, k_1. Note that when $k_1 = 1.9k_2$, the SNR of the reconstructed signal is at its peak.

4.1 The PAPR under transmit power constraint

We present two cases to demonstrate the allocation of power in time-domain to samples of r_n and θ_n and show the effect on the PAPR. In the first case, P_1, the samples of θ_n are set to cover the full dynamic range of the LED, *i.e.* $DR_\theta = DR_{LED}$ (similar to the P-OFDM symbol shown in Fig. 2). However, in the second case, P_2, a power balance approach is considered, where equal power allocation to the r_n and θ_n samples is ensured, *i.e.* $DR_\theta < DR_{LED}$ and k_1 is increased relative to k_2. At the receiver, the allocated powers are recombined during the regeneration of the complex P-OFDM samples in the Cartesian domain. In the upper subplot of Fig. 4, the cumulative distribution function (CDF) plots of the PAPR for P_1 and ACO-OFDM are depicted. Indeed P_1 offers a 2 dB reduction compared to ACO-OFDM for the same number of subcarriers. In the lower subplot of Fig. 4, the CDF plots of the PAPR for P_2 and ACO-OFDM are depicted and the PAPR of P_2 is about 4dB lower compared to ACO-OFDM.

4.2 The induced clipping noise power under transmit power and LED dynamic-range constraint

Using $P_s = 15$dBm, $I_H = 1$A and $I_L = I_{th} = 0$A. The $k_1 r_n$ and $k_2 \theta_n$ sample values beyond DR_{LED} are clipped at I_H. As shown in Fig. 5, the power balance approach (P_2) results in -30dBm induced clipping noise power even at 2dB clipping ratio. However, ACO-OFDM requires 11dB clipping ratio to induce the same amount of clipping noise power, *i.e.* 30dB drop from 0dBm at 2dB clipping ratio.

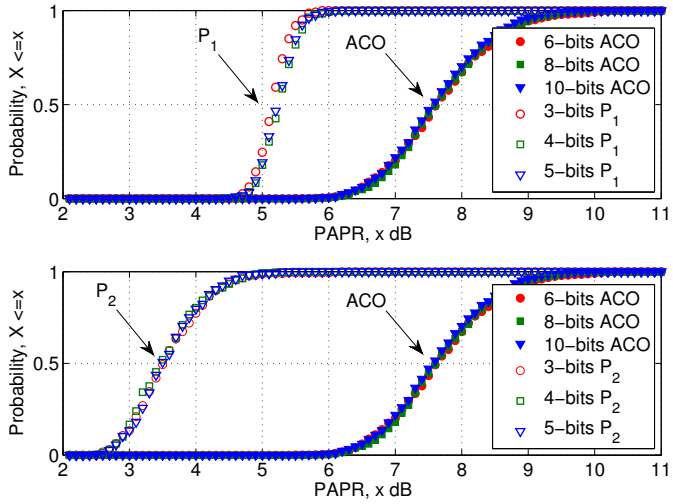

Figure 4: The CDF of the PAPR for ACO-OFDM, P_1 and P_2.

4.3 The BER under transmit power and LED dynamic-range constraint

As shown in Fig. 6 (left), the BER of ACO-OFDM is above the forward error correction (FEC) limit for clipping ratios below 11dB, even at 6-bits per sub-carrier. For P_1 (Fig. 6 (middle), and for the equivalent 3-bits per sub-carrier, the FEC limit is achieved around 7dB clipping ratio. Finally, using P_2 and 3-bits per sub-carrier, a clipping ratio of 2dB supports 5×10^{-5} BER. It is noticed that P_2 greatly improves the BER performance at extremely low clipping ratios and highlights the fact that in future work, we need to investigate BER optimization using adaptive power allocation.

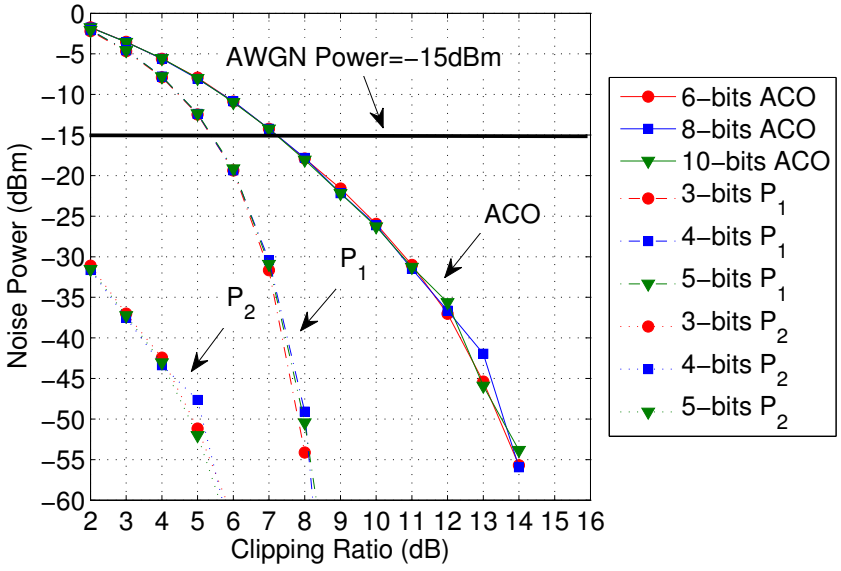

Figure 5: Noise Power vs. Clipping Ratio.

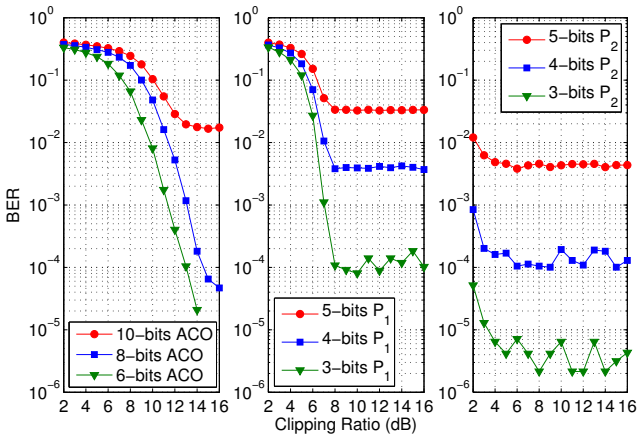

Figure 6: BER vs. Clipping Ratio.

5 Conclusion

We have presented a noise and PAPR analysis of P-OFDM. We have shown that a judicious use of power allocation can lead to an improved receiver SNR. In addition, appropriate allocation of phase versus amplitude power can significantly reduce the effect of intensity clipping on the BER. As shown in Fig. 6, an effective power balance between phase and amplitude reduces the BER by factors of 10. Though P-OFDM is a nonlinear modulation technique, equalization before reconstruction can be used to mitigate the effect of the channel. This method promises high throughput in intensity-limited environments and is a promising method for increasing data rate for data hungry consumers.

References

[1] C. Lin, *Broadband Optical Access, FTTH, and Home Networks–the Broadband Future* (Wiley, 2006).

[2] H. Elgala, R. Mesleh and H. Haas, "Indoor optical wireless communication: potential and state-of-the-art," *Commun. Mag.*, **49**, 9, pp. 56–62 (IEEE, 2011).

[3] J. Armstrong and A. J. Lowery, " Power efficient optical OFDM," *Electronics Letters*, **42**, 6, pp. 370–372 (IET, 2006).

[4] D. Barros, S. K. Wilson and J. M. Kahn, "Comparison of Orthogonal Frequency Division Multiplexing and Pulse-Amplitude Modulation in Indoor Wireless Optical Links," *Trans. Commun.*, **60**, 1, pp. 153–163 (IEEE, 2012).

[5] J. Gancarz, H. Elgala and T. D. C. Little, "Impact of lighting requirements on VLC systems," *Commun. Mag.*, **51**, 12, pp. 34–41 (IEEE, 2013).

[6] E. Vanin, "Performance evaluation of intensity modulated optical OFDM system with digital baseband distortion," *OpEx*, **19**, 5, pp. 4280–4293 (OSA, 2011).

[7] H. Elgala, R. Mesleh and H. Haas, "Non-linearity effects and predistortion in optical OFDM wireless transmission using LEDs," *IJUWBCS*, **1**, 2, pp. 143–150 (Inderscience Publishers, 2009).

[8] H. Elgala, R. Mesleh and H. Haas, "A study of LED nonlinearity effects on optical wireless transmission using OFDM," *IFIP on WOCN*, pp. 1–5 (IEEE, 2009).

[9] N. Fernando, Y. Hong and E. Viterbo, "Flip-OFDM for optical wireless communications," *ITW*, pp. 5–9 (IEEE, 2011).

[10] A. Nuwanpriya, A. Grant, S. W. Ho and L. Luo, "Position modulating OFDM for optical wireless communications," *GC Wkshps*, pp. 1219–1223 (IEEE, 2012).

[11] H. Elgala and T. D. C. Little, "P-OFDM: Spectrally Effcient Unipolar OFDM," *OFC*, Th3G.7 (OSA, 2014).

[12] H. Elgala and T. D. C. Little, "Polar-Based OFDM and SCFDE Links towards Energy-Efficient Gbps Transmission under IM-DD Optical System Constraints," *JOCN*, **7**, 2, pp. A277–A284 (OSA, 2015).